AIP | Journal of Applied Physics

Simulation of multilevel switching in electrochemical metallization memory cells

Stephan Menzel, Ulrich Böttger, and Rainer Waser

Citation: J. Appl. Phys. **111**, 014501 (2012); doi: 10.1063/1.3673239
View online: http://dx.doi.org/10.1063/1.3673239
View Table of Contents: http://jap.aip.org/resource/1/JAPIAU/v111/i1
Published by the American Institute of Physics.

Additional information on J. Appl. Phys.

Journal Homepage: http://jap.aip.org/
Journal Information: http://jap.aip.org/about/about_the_journal
Top downloads: http://jap.aip.org/features/most_downloaded
Information for Authors: http://jap.aip.org/authors

ADVERTISEMENT

Downloaded 15 May 2013 to 134.94.122.141. This article is copyrighted as indicated in the abstract. Reuse of AIP content is subject to the terms at: http://jap.aip.org/about/rights_and_permissions

Simulation of multilevel switching in electrochemical metallization memory cells

Stephan Menzel,[1,a)] Ulrich Böttger,[1] and Rainer Waser[1,2]
[1]Institute of Materials in Electrical Engineering and Information Technology, RWTH Aachen University, 52074 Aachen, Germany
[2]Peter Grünberg Institut, Forschungszentrum Jülich, 52425 Jülich, Germany

(Received 22 July 2011; accepted 22 November 2011; published online 3 January 2012)

We report on a simulation model for bipolar resistive switching in cation-migration based memristive devices. The model is based on the electrochemical driven growth and dissolution of a metallic filament. The origin of multilevel switching is proposed to be direct tunneling between the growing filament and the counter electrode. An important result of our parameter simulation studies is that different materials show the same experimental multilevel behavior. Our model fully reproduces the experimental data and allows for an explanation of the transition from bipolar to nonpolar switching.
© 2012 American Institute of Physics. [doi:10.1063/1.3673239]

I. INTRODUCTION

Memristive devices based on redox processes on the nanoscale have attracted a great deal of attention for their potential use in future nonvolatile memories.[1,2] One potential candidate is electrochemical memory (ECM), which is based on the migration of Cu or Ag cations. Here, the switching is attributed to the electrochemical growth and dissolution of a Cu or Ag nano-sized filament.[3,4] Typically, ECM cells consist of a Cu or Ag active electrode, an ion conducting switching layer (SL), and an inert electrode. The ECM effect has been observed in several materials.[4–8] During the SET process, a positive potential is applied to the active electrode, which is oxidized. Ag or Cu cations are driven out of the active electrode and migrate through the SL. At the inert cathode the cations are reduced and a metallic filament grows toward the anode, resulting in a low resistive state (LRS). This filamentary growth can be attributed to preferred ionic drift path within the SL. In a former study it was also shown that only one filament is responsible for SET operation due to the current compliance.[9] To reset the device to a high resistive state (HRS), the voltage polarity is reversed, leading to the dissolution of the filament. ECM cells show multilevel programming capabilities and strongly nonlinear switching dynamics. In former studies, the origin of this nonlinear switching dynamic was attributed to ion hopping at high electric fields[10,11] or to electron transfer reactions at the electrodes.[9,12] Multilevel programming is often explained as a variation in the width of the conductive filament, resulting in a different LRS.[10,11,13] The LRS can be modulated by an external current compliance (CC) or a load resistor R_L over several orders of magnitude with values above GΩ and below kΩ.[13,14] The resistance of a single-atom contact is about 12.9 kΩ.[15] It is therefore hard to explain the whole range of multilevel states with variation of the filament diameter. A second big issue is connected to the proposed reset mechanism based on a combination of Joule heating and an electrochemical dissolution of the filament.[5] In order to achieve significant Joule heating in thin filaments for typical reset voltages in ECM cells below 0.5 V, reset currents higher than one μA are expected to be necessary.[16,17] For high LRS, however, RESET currents can be less than μA,[2,12,13,18] excluding Joule heating. In addition, nonpolar (unipolar) switching modes also have been demonstrated when the LRS is below 20 kΩ,[5,7,8] which should be covered by a suitable model.

[a)]Author to whom correspondence should be addressed. Electronic mail: menzel@IWE.RWTH-Aachen.de.

II. SIMULATION MODEL

In this work, we report on a continuous 1D physical simulation model to explain bipolar resistive switching in ECM cells based on the modulation of a tunneling gap between the electrochemically growing filament and the counter electrode. Different LRSs in this model are represented by a corresponding tunneling gap, which can be adjusted by an external current compliance. This current control method has been used to fabricate electrode pairs with distinct angstrom-sized gaps.[19] To achieve a 1D model, we approximate the shape of the growing filament as a cylinder with a constant radius. In a microscopic picture, the filament will have some curvature, and deposition might take place at the very top as well as at the sides. Thus the filament radius and the tunneling gap should be regarded as effective parameters, which allows for continuous values.

Figure 1 shows a schematic of the simulation model. The metallic cylindrical filament grows from the inert bottom electrode through the SL and modulates the effective tunneling gap x. Within the SL, ionic and electronic tunneling currents are present. The ionic current path is modeled by two voltage controlled current sources, which represent the electron-transfer reactions at the boundaries (see explanation below) and the resistance due to ionic drift $R_{\mathrm{ion}}(x)$. The electronic current path is attributed to electronic tunneling, represented by one voltage controlled current source. The LRS is reached as the tunneling gap becomes small enough to enable significant tunneling current. The filament

Downloaded 15 May 2013 to 134.94.122.141. This article is copyrighted as indicated in the abstract. Reuse of AIP content is subject to the terms at: http://jap.aip.org/about/rights_and_permissions

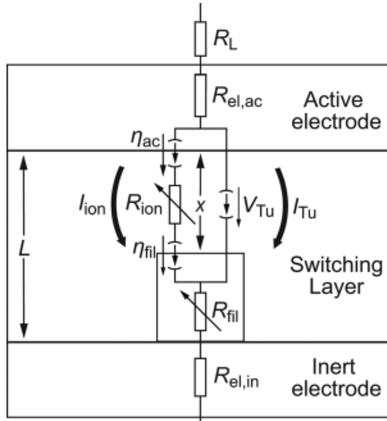

FIG. 1. Schematic of the switching model with equivalent circuit diagram. A switching layer of thickness L is sandwiched between the active top electrode and the inert bottom electrode. A cylindrical filament grows within the SL and modulates the tunneling gap x between filament and active electrode. The elements of the equivalent circuit are an optional load resistor R_L, the electrode resistors $R_{el,ac}$ and $R_{el,in}$, and the filament resistor $R_{fil}(x)$. In the switching layer, the ionic current path (left path) is represented by two voltage controlled current sources with controlling voltages η_{ac} and η_{fil} and the ionic resistance $R_{ion}(x)$. The electronic current path (right path) within the SL is given by one voltage controlled current source with controlling voltage V_{Tu}.

growth/dissolution, and thus the change of x, can be described using Faraday's law,[20,21]

$$\frac{\partial x}{\partial t} = -\frac{M_{Me}}{ze\rho_{m,Me}} J_{Me^{z+}}. \tag{1}$$

Here, J_{Mez+} is the ionic current, z is the charge transfer number, M_{Me} is the atomic mass, and $\rho_{m,Me}$ is the mass density of the deposited metal. In order to simplify the model, the dissolution/growth of the active electrode is neglected, because its active volume is large compared to the volume of the filament. The redox reactions at the electrodes involve an electron transfer reaction. The resulting current density due to this charge transfer is described by the Butler-Volmer equation

$$J_{Me^{z+}} = J_{BV}(\eta) = j_0\left\{\exp\left(\frac{(1-\alpha)ez}{kT}\eta\right) - \exp\left(-\frac{\alpha ez}{kT}\eta\right)\right\} \tag{2}$$

and defines the ionic current.[20] Here, j_0 is the exchange current density, α is the charge transfer coefficient, and η is the overpotential. If η is positive, the left-hand term describing the oxidation process dominates, whereas the second term, describing the reduction process, dominates for negative η. For numerical simplicity, we set $\alpha = 0.5$, and thus Eq. (2) reduces to

$$J_{BV}(\eta) = 2j_0 \sinh\left(\frac{ze}{2kT}\eta\right). \tag{3}$$

For $\eta \gg kT/ze$, Eq. (3) becomes exponentially dependent on η. In a previous study we demonstrated that this nonlinearity can explain the switching dynamics of ECM cells.[9] It should be noted that the Mott-Gurney law[22] describing ion hopping transport shows the same mathematical dependence and thus could also explain the nonlinear switching dynamics. Due to charge neutrality, the ionic currents at the active and the inert electrodes are equal. Therefore, the overpotential at the active electrode–SL interface η_{ac} can be expressed by the filament/SL overpotential η_{fil}, where A_{ac} is the area of the active electrode involved in the redox reaction and A_{fil} is the filament area.

$$\begin{aligned} I_{ion} &= I_{BV}(\eta_{fil}) = I_{BV}(\eta_{ac}) \\ \Leftrightarrow -2j_0A_{fil}\sinh\left(\frac{ze}{2kT}\eta_{fil}\right) &= 2j_0A_{ac}\sinh\left(\left(\frac{ze}{2kT}\eta_{ac}\right)\right) \\ \Rightarrow \eta_{ac} &= \frac{2kT}{ze}\operatorname{arsinh}\left(-\frac{A_{fil}}{A_{ac}}\sinh\left(\frac{ze}{2kT}\eta_{fil}\right)\right). \end{aligned} \tag{4}$$

Note that the algebraic signs of the Butler-Volmer currents in Eq. (4) are different due to the inverse redox reactions occurring at the interfaces. Using Kirchhoff's first law, the cell current is calculated as the sum of the ionic and tunnel currents I_{Tu} in the switching layer as

$$I_{cell} = I_{Tu}(V_{Tu}) + I_{ion} = I_{Tu}(V_{Tu}) + I_{BV}(\eta_{fil}). \tag{5}$$

The tunnel voltage V_{Tu} is equal to the voltage drop across the ionic current path according to Kirchhoff's second law. It can be calculated as the sum of η_{fil}, η_{ac}, and the voltage drop due to the ionic transport in the insulating layer by

$$V_{Tu} = \eta_{ac} - \eta_{fil} + I_{BV}(\eta_{fil})R_{ion}(x) = f(\eta_{fil}, x). \tag{6}$$

The ionic resistance is calculated as $R_{ion} = \rho_{ion}x/A_{ion}$, with the ionic resistivity ρ_{ion} and the effective area of ionic transport within the insulator A_{ion}. For an intermediate voltage range and a trapezoidal barrier, I_{Tu} is calculated according to Simmons[23] as

$$\begin{aligned} I_{Tu} = &\frac{eA_{fil}}{2\pi hx^2}\left(\varphi_0 - \frac{eV_{Tu}}{2}\right)\exp\left(-\frac{4\pi x}{h}\sqrt{2m_{eff}}\sqrt{\varphi_0 - \frac{eV_{Tu}}{2}}\right) \\ &- \frac{eA_{fil}}{2\pi hx^2}\left(\varphi_0 + \frac{eV_{Tu}}{2}\right)\exp\left(-\frac{4\pi x}{h}\sqrt{2m_{eff}}\sqrt{\varphi_0 + \frac{eV_{Tu}}{2}}\right), \end{aligned} \tag{7}$$

where φ_0 is the tunneling barrier height and $m_{eff} = m_r m_0$ is the electron effective mass of the insulating material. In the equivalent circuit diagram, Eq. (7) is represented by a voltage controlled current source, and the controlling voltage is V_{Tu} (see Figure 1). Due to the exponential dependence of I_{Tu} on x, the LRS is very sensitive to small variations in x. For small voltages V_{Tu}, the tunnel junction shows an Ohmic behavior, which is consistent with the experimentally observed characteristic of LRS in ECM cells. Note that a real tunnel barrier has a more parabolic shape and a shorter effective gap.[23] Both effects lead to higher currents than predicted using Eq. (7). The real gaps should thus be larger than in our simulations. Using Eq. (6) with Eq. (7), the tunneling current can be expressed as a function of η_{fil} and x. With Eq. (5), Eq. (6), and Eq. (7), the cell voltage V_{cell} can be calculated using

$$V_{cell} = V_{Tu} + I_{cell}(R_{fil}(x) + R_{el} + R_L) = f(\eta_{fil}, x). \tag{8}$$

Downloaded 15 May 2013 to 134.94.122.141. This article is copyrighted as indicated in the abstract. Reuse of AIP content is subject to the terms at: http://jap.aip.org/about/rights_and_permissions

Here the filament resistance is calculated using $R_{fil} = \rho_{fil} (L - x)/A_{fil}$, where L is the SL thickness. V_{cell} is thus a function of η_{fil} and x. The resistances R_{el} and R_L correspond to the added resistance of both electrodes and an optional load resistor, respectively. Due to the low resistance of the conductive filament and the electrodes, almost the complete cell voltage will drop across the two interfaces and the solid electrolyte. With this set of equations, the switching behavior of ECM can be simulated. For a given V_{cell}, Eq. (1) is solved along with Eq. (8), and in CC Eq. (1) is solved along with Eq. (5). Note that Eq. (5) and Eq. (8) are implicit equations and have to be solved for η_{fil} in each time step in order to solve the ordinary differential equation Eq. (1). This set of equations describes an implicit memristive system.[24] When simulating the SET operation, Eq. (1) is solved along with Eq. (8), as long as the cell current is lower than the current compliance. As soon as CC is reached, Eq. (1) is solved along with Eq. (5) until the end of the SET operation. This differs from real current compliance, which turns back to voltage control as the cell current drops below the SET value.

As a model system for our simulations, we use a cylindrical Cu/SL/Pt structure. Both electrodes have a thickness of 20 nm and a 100 nm radius, which leads to an electrode resistance $R_{el} = 76\,\text{m}\Omega$. R_L is zero in all simulations. The SL thickness is $L = 20$ nm. For numerical simplicity, we set $A_{ion} = A_{ac} = A_{fil} = \pi r_{fil}^2$. Other parameters are $z = 2$, $\rho_{m,Cu} = 8.95\,\text{g/cm}^3$, $M_{Cu} = 1.06 \times 10^{-22}$ g, and $T = 300$ K. The remaining parameters φ_0, m_r, r_{fil}, σ_{ion}, and j_0 depend on the electronic properties of the SL material, its microstructure, and the solubility of Cu ions in the SL. These parameters are varied in our simulations in order to investigate their influence on resistive switching. As reference material in our simulations, we choose SiO_2, and thus $\varphi_{0Cu/SiO2} = 4.2$ eV and $m_{r,SiO2} = 0.86$. The remaining reference values are $\rho_{ion} = 10^{-2}\,\Omega\text{m}$, $j_0 = 10^{-2}\,\text{A/m}^2$, and $r_{fil} = 2$ nm.

III. SIMULATION RESULTS AND DISCUSSION

Figure 2(a) shows the simulated *IV* characteristic (red solid line) using a current compliance of 10 μA. The ECM cell is initially in a HRS. For excitation, a triangular voltage with a 1 V amplitude and 1 s rise time is used (see inset in Fig. 2(a)). The initial 2 s correspond to the SET operation, and the following 2 s to the RESET operation. Obviously, the LRS exhibits an Ohmic behavior, as expected from Eq. (7) for low voltages. During the SET operation, the actual cell voltage is not equal to the applied voltage V_{ap} (blue curve in Fig. 2(a)). As soon as the set CC is reached, V_{cell} drops abruptly. Afterward it decreases gradually during the current control. This behavior can be explained by interpreting the transient data of I_{ion}, I_{Tu}, and x during SET and RESET, shown in Fig. 2(c) and Fig. 2(d), respectively. When V_{ap} is raised, I_{ion} increases according to Eq. (4) and x starts decreasing. This leads to an increase of I_{Tu} (see Eq. (7)), and finally the set CC is reached. A further decrease of x is compensated for by the abrupt drop of V_{cell}. In conclusion, I_{ion} is reduced by three orders of magnitude (see Figure 2(c)), and the filament growth is suppressed. At the end of the SET pulse, a gap of 0.32 nm remains. Note that x still decreases in CC, which allows for a metallic contact at a longer time scale. During RESET, I_{Tu} is orders of magnitude larger than I_{ion} (see Figure 2(d)), but it is very sensitive to x. Thus, even a low ionic current is sufficient to reset the cell. Then, I_{Tu} drops to zero and the filament dissolves completely. The simulation results are in good agreement with the experimental data shown in Fig. 2(b). Note that the field across the remaining gap is very high and can be in the range of dielectric breakdown fields, which should be discussed in terms of reliability and stability of the LRS.

In order to study multilevel programming, we performed simulations with varying CC in which $I_{CC} = I_{SET}$.

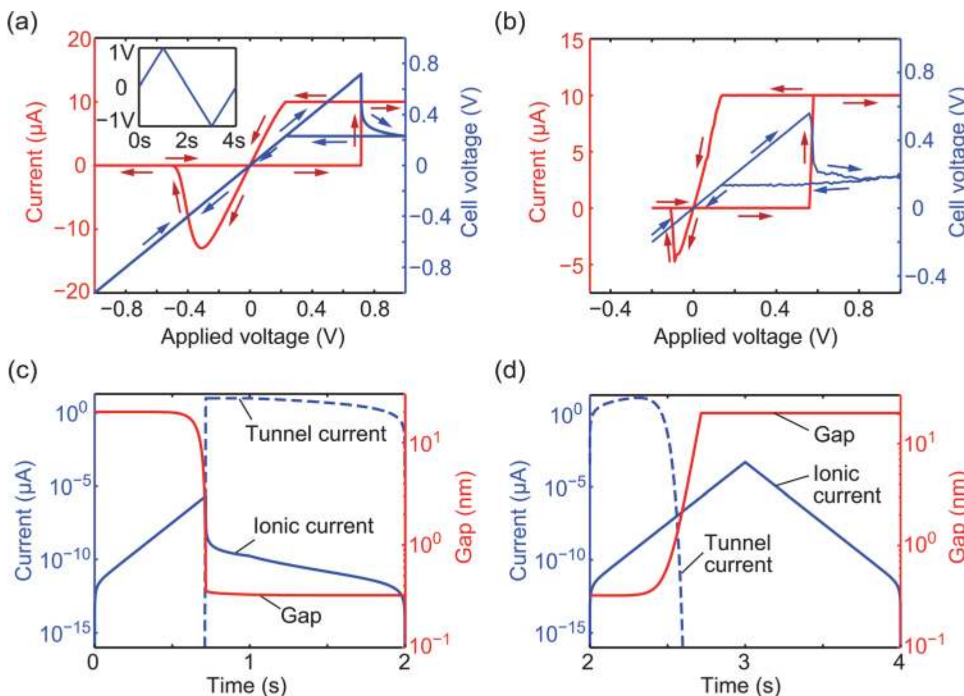

FIG. 2. (Color) (a) Simulated *IV* curve (red) and corresponding relation between V_{cell} and $V_{applied}$ (blue). The applied voltage vs time is shown as an inset. Also shown are the corresponding simulated transient tunneling (dashed blue line), ionic currents (solid blue line), and transient gap (solid red line) during (c) SET and (d) RESET. The absolute values are shown in (d). A gap of 0.32 nm remains after the SET operation. (b) Experimental *IV* characteristic for a $Cu/SiO_2/Pt$ cell (preparation in Ref. 14).

Downloaded 15 May 2013 to 134.94.122.141. This article is copyrighted as indicated in the abstract. Reuse of AIP content is subject to the terms at: http://jap.aip.org/about/rights_and_permissions

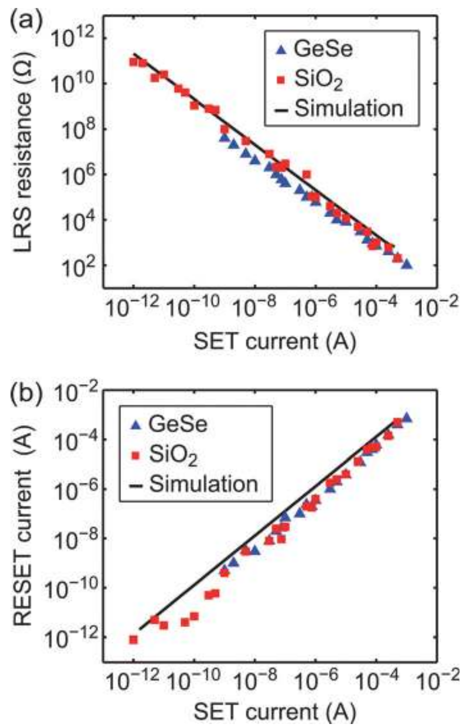

FIG. 3. (Color) (a) LRS resistance vs SET current and (b) corresponding RESET current vs SET current. The simulation results for (a) and (b) are depicted as solid black lines. Experimental data are displayed as blue triangles for a Ag:GeSe system and as red squares for a Cu:SiO_2 system (Ref. 14). The filament radius $r_{fil} = 8$ nm.

Again, a voltage triangle of a 1 V peak voltage with a rise time of 1 s is used, and r_{fil} is set to 8 nm. The simulated LRS values as a function of I_{SET} are shown in Fig. 3(a), along with experimental data. Evidently, the proposed tunneling model is capable of explaining multilevel switching over the full range of SET currents. The remaining gap x_{min} is proportional to $\log(I_{SET})^{-1}$ and changes from 1.10 nm at 1 pA to 0.13 nm at 398 μA. At higher SET currents the gap is closed completely, resulting in a metallic contact. Also, for the relation between RESET and SET, the current experimental data and simulation data are consistent (see Figure 3(b)). Let us now consider how one deposited Cu atom will affect the LRS resistance. As the gap is changed 0.26 nm, the resistance changes by a factor of about 250 according to our simulations. The cylindrical filament area in this simulation consists of approximately 3600 atoms for a filament radius of 8 nm. So, if a single Cu atom is placed on top of this filament, the resistance will change by a factor of approximately 250/3600, which is about 7%. For thinner filaments this factor is higher and discrete resistance steps might occur.

To determine which parameters control the LRS, we performed SET simulation studies with varying reference values for $I_{SET} = 100$ nA, 1 μA, and 10 μA. For each simulation study, only one reference value is varied, and the others are kept constant. For excitation we used 1 ms long 1 V SET pulses with a rise and fall time of 10 ns. This ensures that SET switching occurs during the hold time. Figure 4 shows that the LRS is virtually invariant with the barrier height E_b, the effective mass m_r, and the filament diameter A_{fil}, and it is regulated by I_{SET}. E_b, m_r, and A_{fil} determine x_{min}, as these parameters relate to I_{Tu} (Eq. (7)). With a variation of j_0 of over four orders of magnitude, a small variation of LRS is observed (Fig. 4(c)), whereas x_{min} changes accordingly. This variation is directly related to Eq. (3) and Eq. (1). If j_0 is increased, the growth velocity increases analogously. Thus the CC is reached faster and the filament can grow for a longer time under current control. This leads to a slightly lower LRS resistance. Note that a variation of ρ_{ion} does not change the LRS resistance or x_{min},[25] as the switching speed is limited by the electron transfer reaction.

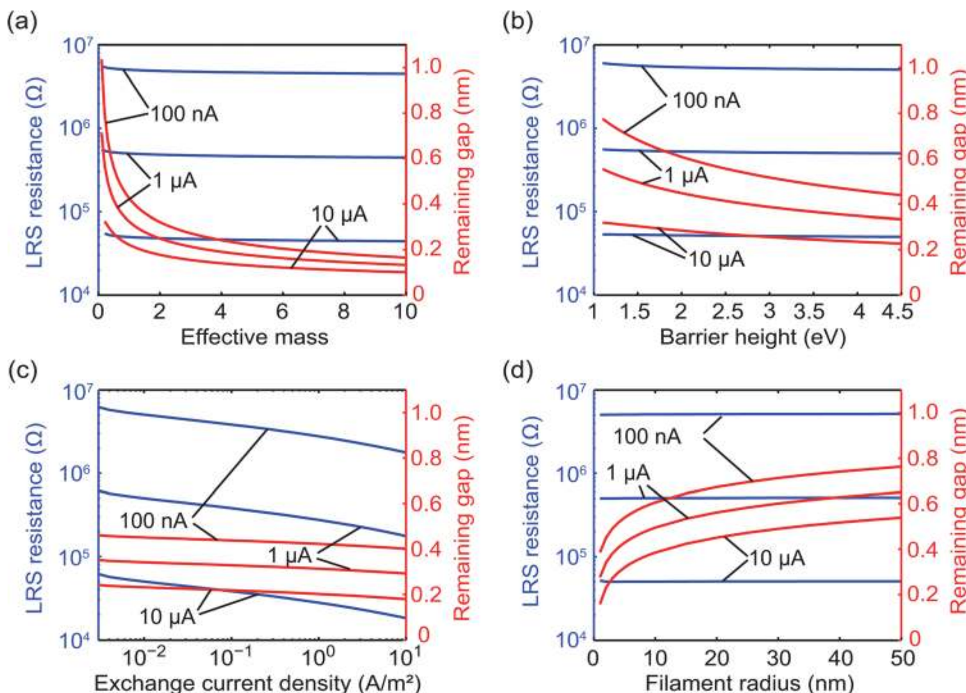

FIG. 4. (Color) LRS resistance (blue lines) and corresponding remaining gap (red lines) vs (a) effective mass, (b) barrier height, (c) exchange current density, and (d) filament radius for SET current levels of 100 nA, 1 μA, and 10 μA.

Downloaded 15 May 2013 to 134.94.122.141. This article is copyrighted as indicated in the abstract. Reuse of AIP content is subject to the terms at: http://jap.aip.org/about/rights_and_permissions

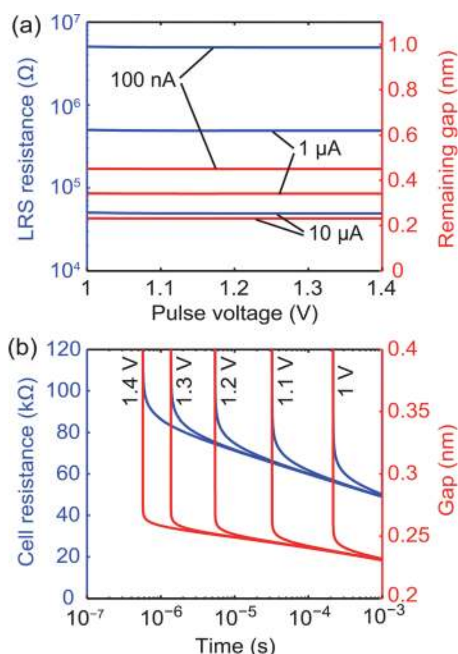

FIG. 5. (Color) (a) LRS resistance (blue) and corresponding remaining gap (red) vs pulse voltage at SET currents of 100 nA, 1 μA, and 10 μA. (b) Transient cell resistance (blue) and gap (red) during the SET pulse for the 10 μA data in (a).

In a further simulation study, the amplitude of the voltage pulse is varied. The simulation results in Fig. 5(a) clearly show that this has no influence on the LRS resistance and, thus, $x_{\min}$. This behavior can be understood by evaluating the transient gap and the cell resistance in Fig. 5(b). Increasing the pulse voltage leads to faster switching, but finally the transient behavior is determined by I_{SET}, which is constant. Interestingly, the initial cell resistance after the switching event is higher for higher voltages. Note that the result of this simulation study differs if a load resistor is used as current compliance. In this case the SET current is given by $I_{\mathrm{SET}} = V_{\mathrm{pulse}}/R_{\mathrm{L}}$, which then controls the LRS.

IV. CONCLUSIONS

In conclusion, we have presented a physical simulation model for resistive switching in ECM cells that gives a remarkably good description of the experimental data. We proposed tunneling as the origin of multilevel switching rather than filament diameter variation, with the LRS level controlled by I_{SET}. In this case its value does not relate to the filament diameter. An important implication of our parameter studies is that different materials show the same experimental multilevel behavior. Small differences in LRS are then attributed to the switching speed of the cell and hence longer growth times. A metallic contact is still possible for a high I_{SET}. This allows for an explanation of the transition from bipolar to nonpolar switching. The former occurs as long as a tunneling gap remains, whereas nonpolar switching occurs for a metallic contact. The material parameters E_{b}, m_{r}, and A_{fil} control the remaining gap, as well as the required I_{SET}, to achieve a metallic contact. Its dissolution might involve Joule heating and thus allows for a nonpolar RESET. For very thin filaments, a resistance jump might occur as the filament achieves a metallic contact. This jump possibly smears out for thick filaments.

[1]D. B. Strukov, G. S. Snider, D. R. Stewart, and R. S. Williams, Nature **453**, 80 (2008).
[2]N. Derhacobian, S. C. Hollmer, N. Gilbert, and M. N. Kozicki, Proc. IEEE **98**, 283 (2010).
[3]R. Waser, R. Dittmann, G. Staikov, and K. Szot, Adv. Mater. **21**, 2632 (2009).
[4]M. Aono and T. Hasegawa, Proc. IEEE **98**, 2228 (2010).
[5]T. Tsuruoka, K. Terabe, T. Hasegawa, and M. Aono, Nanotechnology **21**, 425205 (2010).
[6]R. Waser and M. Aono, Nature Mater. **6**, 833 (2007).
[7]W. Guan, S. Long, Q. Liu, M. Liu, and W. Wang, IEEE Electron Device Lett. **29**, 434 (2008).
[8]C. Schindler, S. C. P. Thermadam, R. Waser, and M. N. Kozicki, IEEE Trans. Electron Devices **54**, 2762 (2007).
[9]S. Menzel, B. Klopstra, C. Kuegeler, U. Boettger, G. Staikov, and R. Waser, Mater. Res. Soc. Symp. Proc. **1160**, 101 (2009).
[10]U. Russo, D. Kamalanathan, D. Ielmini, A. L. Lacaita, and M. N. Kozicki, IEEE Trans. Electron Devices **56**, 1040 (2009).
[11]S. Yu and H.-S. Wong, IEEE Trans. Electron Devices **58**, 1352 (2011).
[12]C. Schindler, G. Staikov, and R. Waser, Appl. Phys. Lett. **94**, 072109 (2009).
[13]Y. Bernard, V. T. Renard, P. Gonon, and V. Jousseaume, Microelectron. Eng. **88**, 814 (2011).
[14]C. Schindler, Resistive switching in electrochemical metallization memory cells (RWTH Aachen, Aachen, Germany, 2009).
[15]E. Scheer, N. Agrait, J. Cuevas, A. Yeyati, B. Ludoph, A. Martin-Rodero, G. Bollinger, J. van Ruitenbeek, and C. Urbina, Nature **394**, 154 (1998).
[16]D. B. Strukov and R. S. Williams, Appl. Phys. A: Mater. Sci. Process. **102**, 851 (2011).
[17]D. Ielmini, F. Nardi, and C. Cagli, Nanotechnology **22**, 254022 (2011).
[18]C. Schindler, M. Meier, R. Waser, and M. N. Kozicki, in *Proceedings of the Non-Volatile Memory Techonology Symposium* (IEEE, New York, 2007), p. 82.
[19]J. Xiang, B. Liu, B. Liu, B. Ren, and Z. Tian, Electrochem. Commun. **8**, 577 (2006).
[20]C. H. Hamann, A. Hamnett, and W. Vielstich, Electrochemistry (Wiley-VCH, Weinheim, 2007).
[21]M. Faraday, Philos. Trans. R. Soc. London **124**, 77 (1834).
[22]N. F. Mott and R. W. Gurney, Electronic processes in ionic crystals (Oxford University Press, London, 1948).
[23]J. G. Simmons, J. Appl. Phys. **34**, 1793 (1963).
[24]L. O. Chua, Appl. Phys. A: Mater. Sci. Process. **102**, 765 (2011).
[25]See supplementary material at http://dx.doi.org/10.1063/1.3673239 for Fig. S1.

Downloaded 15 May 2013 to 134.94.122.141. This article is copyrighted as indicated in the abstract. Reuse of AIP content is subject to the terms at: http://jap.aip.org/about/rights_and_permissions